Experimental demonstration of one-way quantum computation on an ensemble quantum computer

First Author,[1] Second Author,[1] and Third Author[2]

[1]*My Institution*
[2]*Other Institution*

PACS numbers: PACS number

Being entirely different to the traditional quantum circuit model [1] which is based on a network of unitary quantum logic gates, the recently proposed one-way quantum computation model (one-way QC) [2, 3] invokes only a sequence of single-qubit measurements to accomplish the computation, provided a highly entangled state - the cluster state [4] or some other special shaped graph states [5] - is given in advance. This novel quantum computation model has largely broadened people's view on quantum computation, and may lead to a deep understanding on quantum entanglement and measurement. Here, we report the first experimental investigation of the one-way QC in the liquid-state NMR system by demonstrating a two-qubit Deutsch-Josza algorithm. We show that due to the useage of the ensemble quantum computation technology the active feed-forward in one-way QC is not necessary. This is an import result for the future development of one-way quantum computer.

The quantum computer [1], which utilize the laws of quantum physics, is thought to be a powerful computation tool that can beat their classical counterpart on some specific problems [6–8]. Though some pioneer works [9] have revealed its feasibility in a primary step, it is still not very well understood that what are the essential resources that give quantum computer this power. The one-way quantum computation has opened up a possible way which will leads to a further understanding on this important question. The entanglement and measurement are particularly highlighted in this model, thus it is thought that their role in quantum computation would be better understood by further investigating into the one-way QC.

So far, Many works have been done which direct towards a better understanding of the model [5, 10–15]. These include a few experiments which concentrate on the generation and characterization of a few-qubit graph states upon linear optics [11, 12] and a continuous variable system [13], the demonstration of one- and two-qubit gates on a photonic 4-qubit linear cluster state [11, 14], and the realization of a two-qubit search algorithm [11, 14] and a two-qubit Deutsch-Josza algorithm [15] both on the same photonic 4-qubit linear cluster state. Despite the exciting progress these experimental works given, it is still far away to say that we have understood this new quantum computation model very well. The one-way QC is still an open field for both theoretical and practical research.

In this letter, we report the first experimental investigation of the one-way QC in the liquid-state NMR system. We demonstrate a two-qubit Deutsch-Josza algorithm on a star-like 4-qubit graph state (the first one-way based realization of a quantum algorithm on a state other than the 4-qubit linear cluster state). The most remarkable feature which distinguishes our experiment from the former works is the ensemble quantum computing technology used here. As a consequence, we find no active feed-forward (which is a crucial part in the one-way QC to guarantee the determinacy and correctness of the computation) is needed in our experiment, yet the computation is still deterministic and correct. This is entirely different from all known experiments so far [11, 14, 15]. The technical challenges in realizing the active feed-forward are avoided by this unique advantage. Thus this may be an import result for the future development of one-way quantum computer.

Before the introduction to the experiment, we first give a brief review of the Deutsch-Josza (DJ) algorithm [6]. The DJ algorithm is a quantum algorithm that can determine the global property of an unknown function with fewer steps than classical methods. In this letter we consider the simplest version of the DJ algorithm, which determines whether an unknown one-bit to one-bit function f is constant or balanced. There are four possible such functions. Two of them, $f_1(x) = 0$ and $f_2(x) = 1$ $(x = 0, 1)$, are defined as constant functions, while the other two, $f_3(x) = x$ and $f_4(x) = \text{NOT } x$, are balanced functions. To classically accomplish this task one needs to call the function twice to check both the outputs $f(0)$ and $f(1)$. But with DJ algorithm only one function call is needed. The process of the algorithm is illustrated in Fig. 1(a). Initially the two input qubits, a target qubit and a control qubit (denoted by t and c respectively), are both prepared in the state $|+\rangle$ ($|+\rangle = \frac{1}{\sqrt{2}}(|0\rangle + |1\rangle)$ is the eigenstate of the Pauli operator σ_x). Then they are inserted into an oracle which applies the following unitary operations: first a σ_z applied on the target qubit, then the two-qubit operation $|x\rangle_c |y\rangle_t \rightarrow |x\rangle_c |y \oplus f_j(x)\rangle_t$ $(x, y \in \{0, 1\})$ corresponding to the specific funtion f_j $(j = 1, 2, 3, 4)$. The action of the oracle is either preset

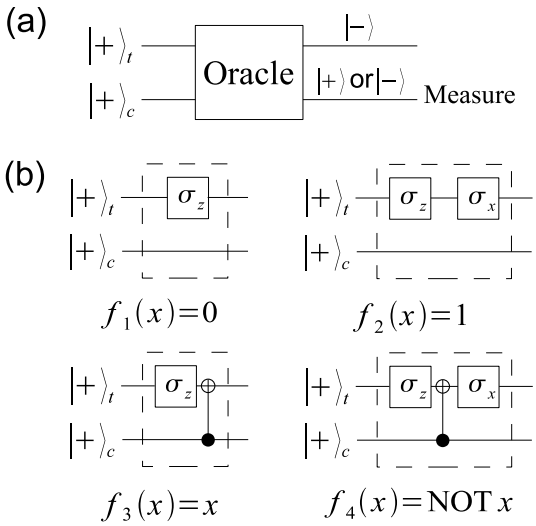

FIG. 1: (a) Schematic illustration of the Deutsch-Josza algorithm. (b) The quantum networks for all possible oracles. The inter-line symbol in the network denotes the controlled-NOT gate $|0\rangle\langle 0|^{(c)}\otimes\mathbb{I}^{(t)}+|1\rangle\langle 1|^{(c)}\otimes\sigma_x^{(t)}$, where the superscripts denote the qubits and $\mathbb{I}$ is identity.

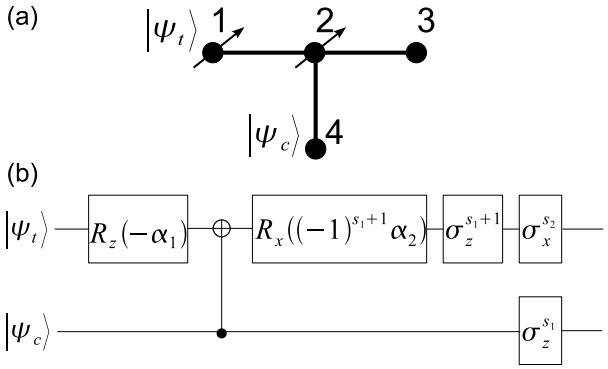

FIG. 2: (a) The star-like 4-qubit graph. The vertices represent the four physical qubits, and each edge between them indicates a controlled-phase gate applied on the connected qubits when to produce the entangled state. The arrows marked on vertices 1 and 2 denote the measurements. For the detailed description of the initial state, entangling, and measurements, see the text. (b) The general logical quantum circuit realized on the above graph with arbitrary logical input states and arbitrary measurement bases. $R_n(\alpha)=e^{-i\alpha\sigma_n/2}$ $(n=x,z)$.

or dictated by the outcome of another algorithm. Finally the control qubit is measured by the operator σ_x. If the outcome is $|+\rangle$ then the function is definitely to be constant, otherwise it is balanced. Fig. 1(b) shows all possible oracles in terms of their quantum networks.

To implement the DJ algorithm one should be able to construct all the possible four configurations. We find it is sufficient to do these on the star-like 4-qubit graph state with appropriate single-qubit measurement sequences and corresponding feed-forwards. In order to clearly describe how we design the measurement sequences, we start with the introduction of the general logical quantum circuit that can be realized on the star-like 4-qubit graph (Fig. 2(a)), with arbitrary logical input states and arbitrary single-qubit measurement bases in the x-y plane. For this purpose, as in Ref. [2], we first prepare the four physical qubits in the graph into the initial state $|\psi_t\rangle_1\otimes|+\rangle_2\otimes|+\rangle_3\otimes|\psi_c\rangle_4$, where the two arbitrary logical input states $|\psi_t\rangle$ and $|\psi_c\rangle$ of the two logical qubits [16] (a target qubit and a control qubit) are initially encoded on the physical qubits 1 and 4. Then all physical qubits are entangled by the entangling operator

$$S=S^{(12)}S^{(23)}S^{(42)}, \tag{1}$$

where $S^{(jk)}=|0\rangle\langle 0|^{(j)}\otimes\sigma_z^{(k)}+|1\rangle\langle 1|^{(j)}\otimes\mathbb{I}^{(k)}$ is a controlled-phase gate applied on the physical qubits j and k [17]. The logical information is now delocalized. It is then manipulated by the measurements carried on the physical qubits 1 and 2 with the bases $B_1(\alpha_1)=\{|\alpha_{1+}\rangle_1,|\alpha_{1-}\rangle_1\}$ and $B_2(\alpha_2)=\{|\alpha_{2+}\rangle_2,|\alpha_{2-}\rangle_2\}$ respectively, where $|\alpha_\pm\rangle=\frac{1}{\sqrt{2}}(|0\rangle\pm e^{i\alpha}|1\rangle)$ and α_1,α_2 are arbitrary angles. After the measurements the logical target qubit is transferred to the physical qubit 3, while the logical control qubit is still encoded on the physical qubit 4. The effective logical quantum circuit performed on the two logical qubits for the above process is shown in Fig. 2(b). The s_1 and s_2 in the circuit denote the outcome of the two measurements, where $s_j=0(1)$ corresponds to the state $|\alpha_{j+}\rangle$ $(|\alpha_{j-}\rangle)$ $(j=1,2)$. The presence of the s_1 and s_2 represents the randomness introduced by the single-qubit measurements, which may make the computation nondeterministic. This can be overcome in the one-way QC by adopting appropriate feed-forward, which means adjusting the future measurement basis according to the outcome of the preceding measurements [2].

The design of the resource entangled state and the single-qubit measurement sequences for implementing the DJ algorithm is done by comparing the general logical circuit in Fig. 2(b) with the networks in Fig. 1(b). Since the input state in the DJ algorithm is $|+\rangle\otimes|+\rangle$, we set $|\psi_t\rangle=|\psi_c\rangle=|+\rangle$. The resulted entangled state, $|\psi_G\rangle=|+\rangle_1|0\rangle_2|-\rangle_3|+\rangle_4+|-\rangle_1|1\rangle_2|+\rangle_3|-\rangle_4$, which is produced by performing the entangling operator S on the initial state $|+\rangle_1\otimes|+\rangle_2\otimes|+\rangle_3\otimes|+\rangle_4$, is exactly the 4-qubit graph state which corresponds to the star-like 4-qubit graph [3] (it is also equivalent to the 4-qubit GHZ state under local unitary operations). The measurement bases and the corresponding feed-forward operations which are chosen to reproduce the networks of all possible oracles are summarized in the Table I. Note in the design of the measurements which correspond to the constant functions f_1 and f_2, the fact is used that a CNOT gate is equivalent to the identity operation when

TABLE I: Measurement bases and feed-forward operations for implementing the DJ algorithm. $\mathrm{FF}^{(3)}$ and $\mathrm{FF}^{(4)}$ represent the feed-forward operations on physical qubits 3 and 4. They can be accounted for by adjusting the measurement basis of the final read-out.

	Measurement bases	$\mathrm{FF}^{(3)}$	$\mathrm{FF}^{(4)}$
f_1	$B_1(0), B_2(0)$	$\sigma_z^{s_1}\sigma_x^{s_2+1}$	$\sigma_z^{s_1}$
f_2	$B_1(0), B_2(0)$	$\sigma_z^{s_1}\sigma_x^{s_2}$	$\sigma_z^{s_1}$
f_3	$B_1(\pi), B_2(0)$	$\sigma_z^{s_1+1}\sigma_x^{s_2}$	$\sigma_z^{s_1}$
f_4	$B_1(\pi), B_2(0)$	$\sigma_z^{s_1+1}\sigma_x^{s_2+1}$	$\sigma_z^{s_1}$

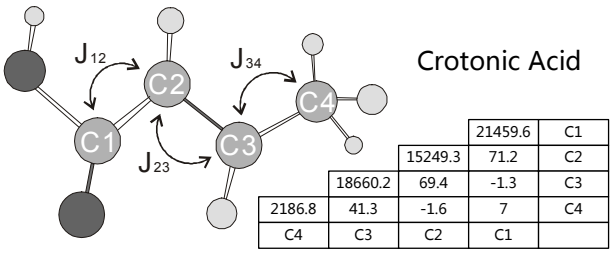

FIG. 3: Molecular structure of crotonic acid with a table of the chemical shifts (on the diagonal) and J-coupling constants (below the diagonal). The parameters are given in unit Hz.

it acts on the state $|+\rangle \otimes |+\rangle$. The final result of the algorithm is read by measuring the physical qubit 4. If its state (after accounting for the feed-forward operation) is $|+\rangle$ ($|-\rangle$) then the function is constant(blanced).

In the experiment we use the spins of the four ^{13}C nuclei in the crotonic acid (Fig. 3) as the four physical qubits. The sample was dissolved in D_2O. The reduced hamiltonian for the four ^{13}C nuclei is written as $H_0 = \sum_{j=1}^{4} \omega_j I_z^{(j)} + 2\pi \sum_{j<k}^{4} J_{jk} I_z^{(j)} I_z^{(k)}$ with the Larmor angular frequencies ω_j and J-coupling strengths J_{jk}. The values of these parameters are listed in Fig. 3.

The experimental generation of the 4-qubit graph state is divided into three steps. Firstly, preparing the pseudopure state $|0000\rangle$ of the four ^{13}C nuclear spins from the thermal equilibrium deviation density matrix $\sum_{j=1}^{4} \sigma_z^{(j)}$. Secondly, preparing the 4-qubit GHZ state $|0\rangle^{\otimes 4} + |1\rangle^{\otimes 4}$ from $|0000\rangle$ by the unitary operation $U_{\mathrm{GHZ}} = \mathrm{CNOT}^{(34)}\mathrm{CNOT}^{(23)}\mathrm{CNOT}^{(12)}\mathrm{H}^{(1)}$, where $\mathrm{H} = \frac{1}{\sqrt{2}}(\sigma_x + \sigma_z)$ is the Hadamard gate. The $\mathrm{CNOT}^{(jk)}$ could be further decomposed into (in time-reversed order)

$$R_y^{(k)}(\frac{\pi}{2}) - e^{-i\frac{\pi}{4}\sigma_z^{(j)}\sigma_z^{(k)}} - R_{-x}^{(k)}(\frac{\pi}{2}) - R_{-z}^{(j)}(\frac{\pi}{2}) - R_{-z}^{(k)}(\frac{\pi}{2}), \quad (2)$$

where $R_y^{(k)}(\frac{\pi}{2}) = e^{-i(\pi/2)\sigma_y^{(k)}/2}$ denotes a $\frac{\pi}{2}$-rotation of the qubit k around the $\hat{y}$ axis, and so forth. The J-coupling gate $e^{-i\frac{\pi}{4}\sigma_z^{(j)}\sigma_z^{(k)}}$ can be realized by the free evolution of the spin system under H_0 with appropriate refocusing operations. Those $\hat{z}$ rotations in CNOT gates can be moved to the beginning of U_{GHZ} by appropriate transformation skills [18], where they are safely annihilated since $\hat{z}$ rotations take no effect on the state $|0000\rangle$. Hence the sequence of the operations is largely simplified. Finally, the 4-qubit graph state $|\psi_{\mathrm{G}}\rangle$ is generated from the GHZ state by the local unitary operations $\mathrm{H}^{(1)}R_{-y}^{(3)}(\frac{\pi}{2})\mathrm{H}^{(4)}$.

The required single-qubit projective measurements in the one-way QC are absent in current NMR quantum computing technologies. But instead we can use the pulsed magnetic field gradients to mimic them [19], whose effect is equivalent to that by applying these projective measurements on every member of the ensemble. For example, one could use the operations (in time-reversed order)

$$P_z^{(1)} = R_{-y}^{(4)}(\pi) - R_{-y}^{(3)}(\pi) - G_1 - R_{-y}^{(4)}(\pi) - R_{-y}^{(2)}(\pi) - G_1 - R_y^{(4)}(\pi) - R_y^{(3)}(\pi) - G_1 - R_y^{(4)}(\pi) - R_y^{(2)}(\pi) - G_1 \quad (3)$$

to mimic the $\sigma_z^{(1)}$ measurement on the physical qubit 1, where G_1 is the pulsed magnetic field gradient along $\hat{z}$ with a period of $\tau_1/4$. These operations dephase all the coherences which are associated with the transitions of qubit 1 in the density matrix $\rho = |\Phi\rangle\langle\Phi|$ (suppose $|\Phi\rangle = |0\rangle_1 |\phi_0\rangle + |1\rangle_1 |\phi_1\rangle$, where $|\phi_{0(1)}\rangle$ is the state of the other three qubits), resulting an ensemble-average density matrix $|0\rangle_1\langle 0| |\phi_0\rangle\langle\phi_0| + |1\rangle_1\langle 1| |\phi_1\rangle\langle\phi_1|$, which is exactly the same as the result by performing projective measurement $\sigma_z^{(1)}$ on every member of the ensemble. To mimic the measurement $\sigma_x^{(1)}$ one just first rotate the qubit 1 to the $\hat{z}$ axis before $P_z^{(1)}$. In our experiment we use the sequences $P_z^{(1)} - R_{-y}^{(1)}(\frac{\pi}{2})$ and $P_z^{(1)} - R_y^{(1)}(\frac{\pi}{2})$ to mimic the measurements with the bases $B_1(0)$ and $B_1(\pi)$ respectively. We left the qubit 1 along $\hat{z}$ after the "measurement" for the purpose that its state could label the "measurement" outcome, i.e., $|0\rangle_1\langle 0|$ denotes $s_1 = 0$ and $|1\rangle_1\langle 1|$ denotes $s_1 = 1$. The measurement on qubit 2 with basis $B_1(0)$ is mimicked by a similar sequence $P_z^{(2)} - R_{-y}^{(2)}(\frac{\pi}{2})$, where

$$P_z^{(2)} = G_2 - R_{-y}^{(4)}(\pi) - R_{-y}^{(1)}(\pi) - G_2 - R_{-y}^{(4)}(\pi) - R_{-y}^{(3)}(\pi) - G_2 - R_y^{(4)}(\pi) - R_y^{(1)}(\pi) - G_2 - R_y^{(4)}(\pi) - R_y^{(3)}(\pi), \quad (4)$$

G_2 is the pulsed magnetic field gradient with a period of $\tau_2/4$ ($\tau_2 \neq \tau_1$).

The randomness associated with projective measurements is avoided by the effective ensemble measurements above. As a consequence, the active feed-forward (i.e., the real-time adjusting of the measurement basis according to the outcome of the preceding measurements during the computation) is not required in our experiment, yet the computation is still deterministic. Since all measurement outcome is recorded in the resulting mixed state, one could choose a sequence of the measurement outcome

in advance to denote in which subspace the computation is actually taken place. Hence all measurement bases can be determined priorly, including all necessary feed-forward. In our experiment we choose this computational subspace as $s_1 = s_2 = 0$. Consequently, in this subspace no feed-forward needs to be accounted for at the read-out stage, since the feed-forward operation $\sigma_z^{s_1}$ on the qubit 4 - the read-out particle - is reduced to identity. (The feed-forward operation on qubit 3 is ignored since it is not the read-out qubit.)

The experiment was implemented on a Bruker Ultra-Shield 500 spectrometer at room temperature. In the practical implementation, all the single-qubit operations above are realized by sequences of strongly modulating NMR pulses [20]. We maximize the gate fidelity of the simulated propagator to the ideal gate, and we also maximize the effective gate fidelity by averaging over a weighted distribution of radio frequency (RF) Field strengths, because the RF-control fields are inhomogeneous over the sample, although it's hard to fully overcome. Theoretically the gate fidelities we calculated for every pulse are greater than 0.99, and the pulse lengths range from 300 to 700 μs.

A full state tomography was performed to the obtained graph state $\rho_{\rm exp}$ (Fig. 4), yielding the fidelity $F = \langle\psi_{\rm G}|\,\rho_{\rm exp}\,|\psi_{\rm G}\rangle = 0.74$. By exploiting the entanglement witness [21] $W = I/2 - |\psi_{\rm G}\rangle\langle\psi_{\rm G}|$ (I denotes identity operatior), one can easily prove the presence of genuine four-partite entanglement here, since a negative expectation value of W is obtained ($\mathrm{Tr}(W\rho_{\rm exp}) = -0.24$). Fig. 5 shows the diagonal elements of the final density matrices of the four particles at the end of the algorithm. The off-diagonal elements were not measured since they are irrelevant to the final readout and are all 0s in theory. Remember the computation is taken place in the subspace $s_1 = s_2 = 0$, thus the algorithm result should be read in the corresponding subspace where particle 1 and 2 are in state $|00\rangle$. The substantial loss in signal intensity arises from decoherence, B1 inhomogeneity effects and imperfect pluses. It shows the fidelity of the network is about 74%, smaller than the expected over 95% for an ideal implementation. Our calculations indicate that in the absence of incoherent effects an overall fidelity of about 85% could be achieved. Nevertheless, our experiment result still shows a good performance of the algorithm when compared with the theoretical expectation.

In conclusion, we have designed and demonstrated an one-way based realization of the DJ algorithm on a star-like four-qubit graph state. This is the first one-way experiment reported which is performed in the liquid-state NMR system and on a state other than the linear four-qubit cluster state. Due to the ensemble quantum computing technology used here, we find no active feed-forward is needed in our experiment yet the computation is still deterministic and correct. This unique and interesting feature avoids the technical challenges in realizing the active feed-forward. Our experimental results are in good agreement with the theoretical expectation.

FIG. 4: (color online). The ideal (a) and measured (b) density matrices of the star-like four-qubit graph state $|+0-+\rangle + |-1+-\rangle$.

[1] M. A. Nielsen and I. L. Chuang, *Quantum Computing and Quantum Information* (Cambridge University Press, Cambridge, England, 2000).

[2] R. Raussendorf and H. J. Briegel, Phys. Rev. Lett. **86**, 5188 (2001).

[3] R. Raussendorf, D. E. Browne, and H. J. Briegel, Phys. Rev. A **68**, 022312 (2003).

[4] H. J. Briegel and R. Raussendorf, Phys. Rev. Lett. **86**, 910 (2001).

[5] M. Van den Nest, A. Miyake, W. Dür, and H. J. Briegel, Phys. Rev. Lett. **97**, 150504 (2006).

[6] D. Deutsch and R. Jozsa, Proc. R. Soc. London A, **439**, 553 (1992).

[7] P. W. Shor, SIAM J. Sci. Stat. Comput. **26**, 1484 (1997).

[8] L. K. Grover, Phys. Rev. Lett. **79**, 325 (1997).

[9] I. L. Chuang, L. M. K. Vandersypen, X. Zhou, D. W. Leung, and S. Lloyd, Nature **393**, 143 (1998); J. A. Jones, M. Mosca, and R. H. Hansen, Nature **393**, 344 (1998); L. M. K. Vandersypen *et al.*, Nature **414**, 883 (2001).

[10] M. A. Nielsen, Phys. Rev. Lett. **93**, 040503 (2004); M. S. Tame, M. Paternostro, M. S. Kim, and V. Vedral, Phys. Rev. A **72**, 012319 (2005); N. Yoran and A. J. Short, Phys. Rev. Lett. **96**, 170503 (2006); D. Gross, K. Kieling, and J. Eisert, Phys. Rev. A **74**, 042343 (2006); V. Danos and E. Kashefi, Phys. Rev. A **74**, 052310 (2006).

[11] P. Walther *et al.*, Nature **434**, 169 (2005).

[12] P. Walther, M. Aspelmeyer, K. J. Resch, and A.

Zeilinger, Phys. Rev. Lett. **95**, 020403 (2005); N. Kiesel *et al.*, Phys. Rev. Lett. **95**, 210502 (2005); A.-N. Zhang *et al.*, Phys. Rev. A **73**, 022330 (2006); C.-Y. Lu *et al.*, Nature Phys. **3**, 91 (2007).
[13] X. Su *et al.*, Phys. Rev. Lett. **98**, 070502 (2007).
[14] R. Prevedel *et al.*, Nature **445**, 65 (2007).
[15] M. S. Tame *et al.*, Phys. Rev. Lett. **98**, 140501 (2007).
[16] A detailed introduction of the logical qubits and physical qubits can be found in [11].
[17] Note that some papers use another controlled-phase gate $S = |0\rangle\langle 0| \otimes \mathbb{I} + |1\rangle\langle 1| \otimes \sigma_z$ as the entangling operator. The produced graph states with these two entangling operators are equivalent up to local unitary operations.
[18] L. M. K. Vandersypen and I. L. Chuang, Rev. Mod. Phys. **76**, 1037 (2005).
[19] G. Teklemariam, E. M. Fortunato, M. A. Pravia, T. F. Havel, and D. G. Cory, Phys. Rev. Lett. **86**, 5845 (2001).
[20] E. M. Fortunato *et al.*, J. Chem. Phys. **116**, 7599 (2002).
[21] G. Tóth and O. Gühne, Phys. Rev. A **72**, 022340 (2005).

FIG. 5: (color online). The measured (color bars) and ideal (dashed bars) diagonal elements of the final density matrices of the four particles. The state of particle 4 in subspace $|0\rangle_1 |0\rangle_2$ represents the algorithm result.